Unconventional Superconductivity in Bilayer Transition Metal Dichalcogenides

Chao-Xing Liu
Department of Physics, The Pennsylvania State University, University Park, Pennsylvania 16802-6300, USA
(Received 23 August 2016; published 21 February 2017)

Bilayer transition metal dichalcogenides (TMDs) belong to a class of materials with two unique features, the coupled spin-valley-layer degrees of freedom and the crystal structure that is globally centrosymmetric but locally noncentrosymmetric. In this Letter, we will show that the combination of these two features can lead to a rich phase diagram for unconventional superconductivity, including intralayer and interlayer singlet pairings and interlayer triplet pairings, in bilayer superconducting TMDs. In particular, we predict that the inhomogeneous Fulde-Ferrell-Larkin-Ovchinnikov state can exist in bilayer TMDs under an in-plane magnetic field. We also discuss the experimental relevance of our results and possible experimental signatures.

DOI: 10.1103/PhysRevLett.118.087001

Introduction.—Unconventional superconductivity [1–3], which is beyond the simple s-wave spin-singlet superconductivity in the Bardeen-Cooper-Schrieffer theory, can emerge in two dimensional (2D) systems, such as surfaces [4–6] or interfaces [7], superconducting heterostructures [8], and 2D or quasi-2D superconducting materials [9–14]. Recently, it was demonstrated that "Ising" superconductivity can exist in monolayer transition metal dichalcogenides (TMDs), such as MoS_2 [11,13] and $NbSe_2$ [12], based on experimental observation that in-plane upper critical field $H_{c2,\parallel}$ is far beyond the paramagnetic limit. The space symmetry group of the monolayer TMD is the D_{3h} group without inversion symmetry. Thus, the monolayer superconducting TMDs belong to the so-called noncentrosymmetric superconductors (SCs) [3], for which spin-up and spin-down Fermi surfaces are split by strong spin-orbit coupling (SOC), leading to a mixing of spin singlet and triplet pairings [15,16]. The existence of triplet components can enhance $H_{c2,\parallel}$ in noncentrosymmetric SCs [17]. In monolayer TMDs, Ising SOC fixes the spin axis along the out-of-plane direction and greatly reduces the Zeeman effect of in-plane magnetic fields, thus, explaining the experimental observations of high $H_{c2,\parallel}$. A high $H_{c2,\parallel}$ was also observed in bilayer TMDs (e.g., $NbSe_2$) [12]. The crystal structure of bilayer TMDs is described by the symmetry group D_{3d} with inversion symmetry, and the corresponding Fermi surfaces are spin degenerate. This experimental result motivates us to study the difference between bilayer superconducting TMDs and conventional SCs.

First, we illustrate the difference from the symmetry aspect. Although inversion symmetry exists in bilayer TMDs, the inversion center should be chosen at the center between two layers, labeled by "P" in Fig. 1(a). As a result, bilayer TMDs belong to a class of materials which are globally centrosymmetric, but locally noncentrosymmetric (for each layer). The absence of local inversion symmetry can lead to "hidden" spin polarization [18,19], spin-layer locking [20,21], and other exotic physical phenomena [22]. The superconductivity for these materials has been studied in the $CeCoIn_5/YbCoIn_5$ hybrid system [10,23], SrPtAs [23–26], and other bilayer Rashba systems [27]. Inhomogeneous Fulde-Ferrell-Larkin-Ovchinikov (FFLO) states were proposed in the $CeCoIn_5/YbCoIn_5$ hybrid system while chiral topological $d+id$ superconductivity was suggested in SrPtAs. Bilayer TMDs possess global D_{3d} symmetry and local D_{3h} symmetry, labeled as $D_{3d}(D_{3h})$, and thus, it is equivalent to that of SrPtAs [25], but different from the $CeCoIn_5/YbCoIn_5$ hybrid system with $D_{3d}(C_{3v})$ symmetry. Because of the D_{3h} symmetry in each layer, Ising SOC is expected in bilayer TMDs and SrPtAs, while Rashba SOC occurs in the $CeCoIn_5/YbCoIn_5$ hybrid system.

In this Letter, we study possible superconducting pairings based on a prototype model of bilayer TMDs. The superconducting phase diagram as a function of intralayer (U_0) and interlayer (V_0) interactions is summarized in Fig. 1(c), in which three different pairings, intralayer A_{1g} pairing, intralayer A_{1u} pairing, and interlayer E_u pairing can exist, depending on the strength and sign of U_0 and V_0. We study the stability of these superconducting pairings under external magnetic fields. In particular, we predict the FFLO state with a finite momentum pairing [28,29] induced by the orbital effect of in-plane magnetic fields.

Phase diagram of bilayer TMDs.—A prototype model for TMDs [15,16,30] was first derived for the conduction band of MoS_2 and can also be applied to other TMDs. This model is constructed on a triangle lattice of Mo atoms with $4d_{z^2}$ orbitals for each monolayer. The conduction band minima appear at two momenta $\pm K$, and one can regard $\pm K$ as a valley index and expand the tight-binding model around $\pm K$ for each layer, as described in Refs. [15,16]. We extend this model to bilayer TMDs by including a layer index. Let us label the annihilation fermion operator as $c_{\sigma,\eta}$, where $\sigma=\uparrow,\downarrow$ is for spin and $\eta=\pm$ is for two layers.

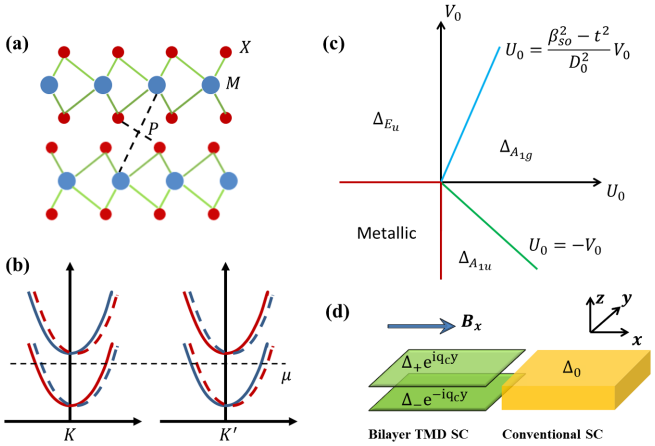

FIG. 1. (a) Crystal structure of bilayer TMDs MX_2 with the inversion center labeled by P. (b) Schematics for energy dispersion of bilayer TMDs where red and blue are for spin-up and spin-down, and solid and dashed lines are for the top and bottom layers. Here, each band is doubly degenerate and we shift the dashed lines a little for the view. (c) The phase diagram as a function of U_0 and V_0. The red, blue, and green lines are the phase boundary, separating three superconducting phases, the A_{1g}, A_{1u}, and E_u pairings, and the metallic phase. (d) Experimental setup of bilayer TMD SC/conventional SC junction.

On the basis of $(c_{\uparrow,+}, c_{\downarrow,+}, c_{\uparrow,-}, c_{\downarrow,-})$, the effective Hamiltonian is

$$\hat{H}_0(\mathbf{p} = \epsilon\mathbf{K} + \mathbf{k}) = \xi_k + \epsilon\beta_{\mathrm{SOC}} s_z \tau_z + t\tau_x, \qquad (1)$$

where s and τ are two sets of Pauli matrices for spin and layer degrees, $\epsilon = \pm$ is for the valley index, and $\xi_k = (\hbar^2/2m)k^2 - \mu$ with chemical potential μ. Here, the β_{SOC} term is the Ising SOC while the t term is the hybridization between two layers. The eigenenergy is given by $\varepsilon_{s,\lambda} = \xi_k + \lambda D_0$ with $D_0 = \sqrt{\beta_{\mathrm{SOC}}^2 + t^2}$ and $s, \lambda = \pm$.s does not appear, and thus, the eigenstates with opposite s are degenerate, as shown in Fig. 1(b). Next, we consider the symmetry classification of superconducting pairings, similar to that in Cu doped Bi_2Se_3 SCs [31] since both materials belong to D_{3d} group. We only consider s-wave pairing, and thus, the gap function $\hat{\Delta}$ is independent of momentum and can be expanded in terms of s and τ ($\hat{\Delta} = \sum_{i,\mu} \Delta_{i,\mu} \gamma_{i,\mu}$ where $\gamma_{i,\mu}$ is a 4×4 matrix composed of s and τ, and i, μ are the indices labeling different representations). Because of the anticommutation relation between fermion operators, the gap function needs to be antisymmetric, and thus, only six matrices s_y, $s_y\tau_x$, $s_y\tau_z$, τ_y, $s_x\tau_y$, $s_z\tau_y$ can couple to s-wave pairing. The classification of these representation matrices, as well as their explicit physical meanings, are listed in Table I, from which $\Delta_{A_{1g},1}$ and $\Delta_{A_{1u}}$ describe intralayer singlet pairings, $\Delta_{A_{1g},2}$ and $\Delta_{A_{2u}}$ give interlayer singlet pairings, while $\Delta_{E_u,1}$ and $\Delta_{E_u,2}$ are interlayer triplet pairings. The pairing interaction can also

TABLE I. The matrix form and the explicit physical meaning of Cooper pairs in the representations A_{1g}, A_{1u}, A_{2u}, and E_u of the D_{3d} group. Here, $c_{\sigma\eta}$ is electron operator with $\eta = \pm$ for layer index and σ for spin. s and τ are Pauli matrices for spin and layer.

Representation		Matrix form	Explicit form
A_{1g}:	$\Delta_{A_{1g},1}$	s_y	$c_{\uparrow+}c_{\downarrow+} + c_{\uparrow-}c_{\downarrow-}$
	$\Delta_{A_{1g},2}$	$s_y\tau_x$	$c_{\uparrow+}c_{\downarrow-} + c_{\uparrow-}c_{\downarrow+}$
A_{1u}: $\Delta_{A_{1u}}$		$s_y\tau_z$	$c_{\uparrow+}c_{\downarrow+} - c_{\uparrow-}c_{\downarrow-}$
A_{2u}: $\Delta_{A_{2u}}$		$s_x\tau_y$	$c_{\uparrow+}c_{\downarrow-} - c_{\uparrow-}c_{\downarrow+}$
E_u:	$\Delta_{E_u,1}$	τ_y	$c_{\uparrow+}c_{\uparrow-}$
	$\Delta_{E_u,2}$	$s_z\tau_y$	$c_{\downarrow+}c_{\downarrow-}$

be decomposed into different pairing channels as $V_{A_{1g},1} = V_{A_{1u}} = (U_0/2)$ and $V_{A_{1g},2} = V_{A_{2u}} = V_{E_u,1} = V_{E_u,2} = (V_0/2)$ (See Supplemental Material [32] for details).

Possible superconducting pairings are studied based on the linearized gap equations [1–3] (See Supplemental Material [32]). Around the valley K (or $-K$), the Fermi surfaces for two spin states in each layer are well separated by the Ising SOC β_{SOC} term. Therefore, below, we assume the Fermi energy only crosses the lower energy band at each valley [Fig. 1(b)] for simplicity. The pairings with different representations do not couple to each other, and thus, we can compute the critical temperature T_c in each representation, separately. The critical temperature normally takes the form $kT_{c0,i} = \frac{2\gamma\omega_D}{\pi} \exp[-(1/N_0 V_{i,\mathrm{eff}})]$, with the representation index i, density of states N_0, the Debye frequency ω_D, and $\gamma \approx 1.77$. The effective interaction is given by $V_{A_{1g},\mathrm{eff}} = 2U_0 + 2V_0(t^2/D_0^2)$ for the A_{1g} pairing, $V_{A_{1u},\mathrm{eff}} = 2U_0(\beta_{\mathrm{SOC}}^2/D_0^2)$ for the A_{1u} pairing, and $V_{E_u,\mathrm{eff}} = 2V_0(\beta_{\mathrm{SOC}}^2/D_0^2)$ for the E_u pairing, from which the corresponding critical temperature in each channel can be determined. The A_{2u} pairing does not exist because $V_{A_{2u},\mathrm{eff}} = 0$. The phase diagram can be extracted by comparing different $T_{c0,i}$ [Fig. 1(c)]. The A_{1g} pairing is favored by strong attractive intralayer interaction ($U_0 > 0$), while the E_u pairing is favored by strong attractive interlayer interaction ($V_0 > 0$). These two phases are separated by the critical line $U_0 = (\beta_{\mathrm{SOC}}^2 - t^2)V_0/D_0^2$. The A_{1u} pairing appears when the repulsive interlayer interaction is stronger than the attractive intralayer interaction ($-V_0 > U_0 > 0$) because repulsive interlayer interaction will favor opposite phases of pairing functions between two layers. The A_{1u} phase is separated from the A_{1g} phase by a critical line $U_0 = -V_0$. When both U_0 and V_0 are repulsive interaction ($U_0, V_0 < 0$), no superconductivity can exist. For the 2D E_u pairing, $\Delta_{E_u,1}$ and $\Delta_{E_u,2}$ are degenerate. By taking into account the fourth order term in the Landau free energy (See Supplemental Material [32]), either nematic superconductivity $(\Delta_{E_u,1}, \Delta_{E_u,2}) = \Delta_{E_u}(\cos\theta, \sin\theta)$ (θ is a constant) [34] or chiral superconductivity with $(\Delta_{E_u,1}, \Delta_{E_u,2}) = \Delta_{E_u}(1, i)$ can be stabilized [35].

Magnetic field effect.—Next, we study the effect of magnetic fields on bilayer superconducting TMDs. Generally, magnetic fields have two effects, the Zeeman effect and the orbital effect. The Zeeman coupling is given by

$$\hat{H}_{\mathrm{Zee}} = g\mathbf{B}\cdot\mathbf{s}, \tag{2}$$

where $\mathbf{B}$ labels the magnetic field, and the Bohr magneton is absorbed into g factor. The orbital effect is normally included by replacing the momentum $\mathbf{k}$ in ξ_k with the canonical momentum $\boldsymbol{\pi} = \mathbf{k} + (e/\hbar)\mathbf{A}$ with vector potential $\mathbf{A}$ (Peierls substitution). The orbital effect of in-plane magnetic fields is normally not important for a quasi-2D system. However, that is not the case in bilayer TMDs due to its unusual band structure. Let us choose $\mathbf{A} = (0, -B_x z, 0)$ for the in-plane magnetic field B_x, in which the origin $z = 0$ is located at the center between two layers. As a result, ξ_k is changed to $\xi_\pi = (\hbar^2/2m)\{k_x^2 + [k_y - (eB_x z_0/2\hbar)\tau_z]^2\} - \mu$ after the substitution, where z_0 is the distance between two layers.

The Ginzburg-Landau free energy is constructed as

$$L = \frac{1}{2}\sum_{\mathbf{q},i\mu,j\nu}\Delta^*_{i,\mu}(\mathbf{q})\left(\frac{1}{V_i}\delta_{ij}\delta_{\mu\nu} - \chi^{(2)}_{ij,\mu\nu}(\mathbf{q},\mathbf{B})\right)\Delta_{j,\nu}(\mathbf{q}) + L_4, \tag{3}$$

where L_4 describes the fourth order term. The superconductivity susceptibility $\chi^{(2)}_{ij,\mu\nu}$ can be expanded up to the second order of $\mathbf{q}$ and $\mathbf{B}$ (q_iq_j, B_iB_j and q_iB_j with $i, j = x, y, z$). The magnetic field correction to $T_{c0,i}$ for different pairings can be extracted by minimizing the above free energy (See Supplemental Material [32]).

Because of the orbital effect, the Hamiltonian (1) is changed to

$$\hat{H}_0' = \xi_k - \hbar v_Q k_y \tau_z + \epsilon\beta_{\mathrm{SOC}} s_z\tau_z + t\tau_x, \tag{4}$$

where $v_Q = (eB_x z_0/2m)$, and the chemical potential μ in ξ_k is redefined to include the B_x^2 term. First, we focus on the limit $t \to 0$, in which the energy dispersion of the Hamiltonian (4) is shown in Fig. 2(a). The energy bands on the top and bottom layers are shifted in the opposite directions in the momentum space by $Q = (eB_x z_0/2\hbar)$. This momentum shift cannot be "gauged away," and thus, the intralayer spin-singlet pairing must carry a nonzero total momentum. This immediately suggests the possibility of the FFLO state [28,29,36] for the intralayer singlet A_{1g} and A_{1u} pairings. Since in-plane magnetic fields break the D_{3d} symmetry, the orbital effect can mix the singlet A_{1g} and A_{1u} pairings. In the limit $t \to 0$ with $T_{c0,A_{1g}} = T_{c0,A_{1u}} = T_{c0}$, we derive the free energy for the coupled A_{1g} and A_{1u} pairings as

$$L_2 = \frac{1}{2}\sum_{\mathbf{q}}\left\{\left[4N_0 ln\left(\frac{T}{T_{c0}}\right) - \mathcal{P}(h_x,\mathbf{q})\right]\sum_{i=A_{1g},A_{1u}}|\Delta_i|^2 - \Delta^*_{A_{1g}}\mathcal{Q}\Delta_{A_{1u}} - \Delta^*_{A_{1u}}\mathcal{Q}\Delta_{A_{1g}}\right\}, \tag{5}$$

in which the detailed form of $\mathcal{P}$ and $\mathcal{Q}$ are defined in the Supplemental Material [32]. The term $\mathcal{Q} = \tilde{K}B_x q_y$ with a constant $\tilde{K}$ mixes A_{1g} and A_{1u} pairings. With a transformation $\Delta_\pm = (1/\sqrt{2})(\Delta_{A_{1g}} \pm \Delta_{A_{1u}})$, the free energy is changed to

$$L_2 = \frac{1}{2}\sum_{\alpha=\pm,\mathbf{q}}\left[4N_0\ln\left(\frac{T}{T_{c0}}\right) - \mathcal{P}(B_x,\mathbf{q}) - \alpha\mathcal{Q}(B_x,\mathbf{q})\right]|\Delta_\alpha|^2. \tag{6}$$

The corresponding critical temperature is determined by maximizing $\ln(T_c/T_{c0}) = (1/4N_0)[\mathcal{P}(B_x,\mathbf{q}) + \alpha\mathcal{Q}(B_x,\mathbf{q})]$ with respect to $\mathbf{q}$ and α. From the explicit form of $\mathcal{P}$ and $\mathcal{Q}$, the maximum is achieved by $q_x = 0$ and $|q_y| = q_c = (eB_x z_0/\hbar) = 2Q$, thus, realizing the FFLO state. The corresponding correction to T_c vanishes ($T_c = T_{c0}$). As a comparison, the T_c of zero momentum pairing decreases with magnetic fields as $\ln(T_c(\mathbf{q}=0)/T_{c0}) = -C(\hbar v_Q k_f/2\pi kT)^2 \propto -B_x^2$, and the FFLO state is always favored in the limit $t \to 0$ for in-plane magnetic fields.

The form of the stable pairing function depends on the sign of $\mathcal{Q}$. Let us assume $B_x > 0$ and $\tilde{K} > 0$ in $\mathcal{Q} = \tilde{K}B_x q_y$. If $q_y = q_c > 0$, $\mathcal{Q} > 0$, and thus, Δ_+ pairing is favored. If $q_y = -q_c < 0$, $\mathcal{Q} < 0$, and Δ_- is favored. $\Delta_+(q_c)$ and $\Delta_-(-q_c)$ are degenerate for the second order term of free energy. The FFLO state in the real space is

$$\Delta(\mathbf{r}) = \Delta_+(q_c)e^{iq_c y} + \Delta_-(-q_c)e^{-iq_c y}. \tag{7}$$

The exact form of pairing function is determined by the fourth order term of $\Delta_+(q_c)$ and $\Delta_-(-q_c)$, which is phenomenologically given by

$$L_4 = \mathcal{B}_s(|\Delta_+(q_c)|^2 + |\Delta_-(-q_c)|^2)^2 + \mathcal{B}_a(|\Delta_+(q_c)|^2 - |\Delta_-(-q_c)|^2)^2. \tag{8}$$

If $\mathcal{B}_a > 0$, we need $|\Delta_+(q_c)| = |\Delta_-(-q_c)| = \Delta_0$ to minimize L_4. This state is known as the LO phase [28,37], stripe phase [4,6,8,38], or pair density wave [10,39,40]. If $\mathcal{B}_a < 0$, we have either $\Delta_+(q_c) = 0$ or $\Delta_-(-q_c) = 0$. In either case, the amplitude of $\Delta(\mathbf{r})$ is fixed while its phase oscillates, thus, corresponding to the FF phase [29,37] or helical phase [3,38,41–43]. In the limit $t \to 0$, the coefficients are computed as $\mathcal{B}_s = \mathcal{B}_a = (7N_0\zeta(3)/16(\pi kT_{c0})^2) > 0$. Therefore, the stripe phase will be favored under an in-plane magnetic field near the critical temperature.

In the limit $t \to 0$, Δ_+ and Δ_- are just the singlet pairing on the top and bottom layers according to Table I, and the

free energies for Δ_+ and Δ_- become decoupled [see Eq. (6) for L_2 term and Eq. (96) of the Supplemental Material [32] for L_4 term]. Thus, the FFLO state in Eq. (7) can be viewed as two independent helical phases in two separate layers. No supercurrent or other observables can exist in helical phases [41,42] for infinite large systems. To identify this phase, one needs to consider a Josephson junction structure between bilayer TMDs and conventional SCs [Fig. 1(d)], similar to that discussed in Refs. [3,42,44] (See Supplemental Material [32] for details). For a finite tunneling t, the interference between two layers leads to the gap oscillation of the stripe phase in Eq. (7).

We notice that the FFLO phase has been proposed in noncentrosymmetric SCs under a magnetic field [6,23], and emphasize two essential differences between our case and noncentrosymmetric SCs. (1) In noncentrosymmetric SCs, the FFLO phase is induced by a linear gradient term $\tilde{K}_{ij}\Delta^* B_i q_j \Delta$ ($\tilde{K}_{ij}$ is a parameter) that breaks inversion symmetry. In contrast, inversion symmetry is preserved in our system, and the linear gradient term ($\tilde{K}_{ij}\Delta^*_{A_{1g}} B_i q_j \Delta_{A_{1u}}$) couples two pairings with opposite parities. (2) In noncentrosymmetric SCs, the FFLO phase results from the combination of Rashba SOC and the Zeeman effect of magnetic fields. In our system, the FFLO phase is from the combination of Ising SOC and the orbital effect of magnetic fields. In particular, this phase can occur for any magnetic field strength in the weak interlayer coupling limit $t \to 0$.

When $t \neq 0$, the occurrence of the FFLO phase will be shifted to a finite magnetic field. We numerically minimize free energy with respect to the momentum $\mathbf{q}$ and calculate the magnetic field correction to T_c. In Fig. 2(b), T_c/T_{c0} is plotted as a function of magnetic field B_x for three hybridization parameters t. The momenta for the corresponding stable states, labeled by q_c, are shown in Fig. 2(c). For a weak hybridization ($t = 1$ meV $\ll \beta_{so} = 40$ meV), the FFLO phase appears at a small B_x, and the corresponding q_c approaches $2Q$ with increasing B_x. There is only a weak correction to T_c for the FFLO phase [black line in Fig. 2(b)]. When increasing hybridization ($t = 5$, 10 meV), zero momentum pairing is favored for small B_x and leads to a rapid decrease of T_c with its correction given by $(T_c - T_{c0})/T_{c0} \propto -B_x^2$ [red and blue lines in Fig. 2(b)]. When B_x becomes larger, a transition from zero momentum pairing to the FFLO state occurs. The decreasing in T_c deviates from the B_x^2 dependence and becomes weaker. Experimentally, one can control the hybridization between two layers by inserting an insulating layer in between, and the deviation of the T_c correction from the B_x^2 dependence implies the occurrence of FFLO states in this system. We construct the phase diagram further by evaluating gap functions as a function of temperatures and magnetic fields for $t = 10$ meV in Fig. 2(d). As discussed in the Supplemental Material [32], the transition from the normal metal [III region in Fig. 2(d)] to uniform SC (I region) or

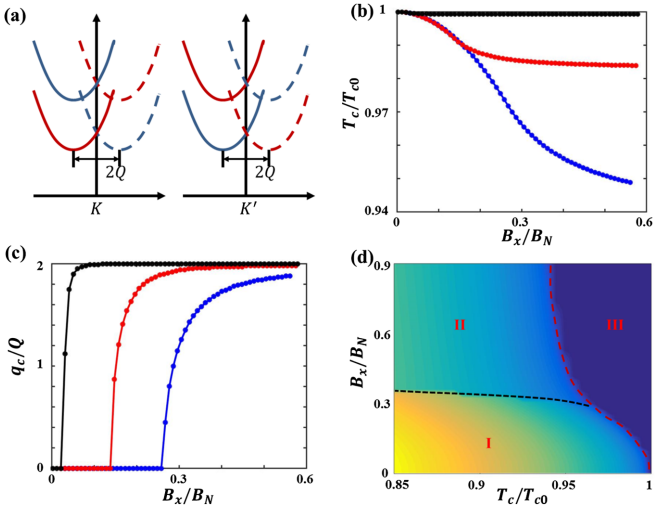

FIG. 2. (a) Schematics of energy dispersion for bilayer TMDs with an in-plane magnetic field. Here, red and blue colors are for opposite spins and solid and dashed lines are for top and bottom layers. (b) The magnetic field dependence of the critical temperature T_c. Here, the black line is for $t = 1$ meV, the red line is for $t = 5$ meV, while the blue is for $t = 10$ meV. Other parameters are chosen as $\beta_{\mathrm{SOC}} = 40$ meV, $\hbar v_F = 30$ meV$\cdot$nm and $m = 0.6m_e$ with electron mass m_e, $N_0U_0 = 0.3$ and $N_0V_0 = 0.1$. Only the orbital effect is taken into account. (c) The momentum q_c for the stable pairing state as a function of B_x. (d) Phase diagram as a function of B_x and T_c. Here, I is for conventional SC phase, II is for FFLO state, and III is for normal metal. $B_N = (2kT_{c0}/v_f z_0)$.

FFLO state (II region) is of the second order type [dashed red line in Fig. 2(d)] while the transition between uniform SC and the FFLO state is of the first order type [dashed black line in Fig. 2(d)].

Besides the orbital effect, the correction of T_c due to the Zeeman effect, which is the same for zero-momentum pairing and the FFLO phase, is given by $\ln(T_{c,A_{1g}}/T_{c0,A_{1g}}) \propto -(t^2/\beta_{\mathrm{SOC}}^2)B_x^2$ for the A_{1g} pairing and $\ln(T_{c,A_{1g}}/T_{c0,A_{1g}}) \propto -(t^4/\beta_{\mathrm{SOC}}^4)B_x^2$ for the A_{1u} pairing. Additional factors $t^2/\beta_{\mathrm{SOC}}^2$ and $t^4/\beta_{\mathrm{SOC}}^4$ greatly reduce the B_x^2 dependence for the A_{1g} and A_{1u} pairings in the limit $t \ll \beta_{\mathrm{SOC}}$. The behavior of the out-of-plane magnetic field (B_z) in bilayer TMDs is similar to that of conventional SCs (See Supplemental Material [32]).

Discussion and conclusion.—In realistic bilayer superconducting TMDs, the Fermi energy will cross both spin states in each layer. However, once the Ising SOC is larger than other energy scales ($\beta_{\mathrm{SOC}} \gg t$, $\hbar k_f v_Q$, $\hbar v_f q$), the Fermi surfaces for two spin states in one layer are well separated and the physics discussed here should be valid qualitatively. Based on the existing experiments, the A_{1g} pairing is most likely to exist at a zero magnetic field. In this case, we predict the occurrence of the FFLO phase under an in-plane magnetic field. The onset magnetic field is determined by the ratio between interlayer hybridization

t and Ising SOC β_{SOC} ($(t/\beta_{\mathrm{SOC}}) \sim 0.27$ in $NbSe_2$) [12]. Our results suggest a weak correction to T_c for both the orbital and Zeeman effects of in-plane magnetic fields, thus, consistent with experimental observations of high in-plane critical fields in bilayer superconducting TMDs [12]. The central physics in this Letter originates from the unique crystal symmetry property, and similar physics can occur in SrPtAs [25]. Similar physics also occurs for exciton condensate in a bilayer system [45,46]. Our work paves a new avenue to search for unconventional superconductivity in 2D centrosymmetric SCs.

We would like to thank Xin Liu, K. T. Law, and Kin Fai Mak for the helpful discussions. C.-X. L. acknowledges support from Office of Naval Research (Grant No. N00014-15-1-2675). C.-X. L. also acknowledges the Pennsylvania State University Two-Dimensional Crystal Consortium – Materials Innovation Platform (2DCC-MIP) which is supported by NSF cooperative Agreement No. DMR-1539916.

[1] M. Sigrist and K. Ueda, Rev. Mod. Phys. **63**, 239 (1991).
[2] V. P. Mineev and K. Samokhin, *Introduction to Unconventional Superconductivity* (Gordon and Breach Science Publishers, Amsterdam, 1999).
[3] E. Bauer and M. Sigrist, *Non-Centrosymmetric Superconductors: Introduction and Overview* (Springer Science and Business Media, Berlin, 2012), Vol. 847.
[4] O. V. Dimitrova and M. V. Feigelman, JETP Lett. **78**, 637 (2003).
[5] D. Agterberg, Physica (Amsterdam) **387C**, 13 (2003).
[6] V. Barzykin and L. P. Gorkov, Phys. Rev. Lett. **89**, 227002 (2002).
[7] K. Aoyama and M. Sigrist, Phys. Rev. Lett. **109**, 237007 (2012).
[8] T. Yoshida, M. Sigrist, and Y. Yanase, J. Phys. Soc. Jpn. **82**, 074714 (2013).
[9] M. Houzet, A. Buzdin, L. Bulaevskii, and M. Maley, Phys. Rev. Lett. **88**, 227001 (2002).
[10] T. Yoshida, M. Sigrist, and Y. Yanase, Phys. Rev. B **86**, 134514 (2012).
[11] J. Lu, O. Zheliuk, I. Leermakers, N. F. Yuan, U. Zeitler, K. T. Law, and J. Ye, Science **350**, 1353 (2015).
[12] X. Xi, Z. Wang, W. Zhao, J.-H. Park, K. T. Law, H. Berger, L. Forró, J. Shan, and K. F. Mak, Nat. Phys. **12**, 139 (2015).
[13] Y. Saito, Y. Nakamura, M. S. Bahramy, Y. Kohama, J. Ye, Y. Kasahara, Y. Nakagawa, M. Onga, M. Tokunaga, T. Nojima *et al.*, Nat. Phys. **12**, 144 (2016).
[14] E. Navarro-Moratalla, J. O. Island, S. Mañas-Valero, E. Pinilla-Cienfuegos, A. Castellanos-Gomez, J. Quereda, G. Rubio-Bollinger, L. Chirolli, J. A. Silva-Guillén, N. Agraït *et al.*, Nat. Commun. **7**, 11043 (2016).
[15] B. T. Zhou, N. F. Q. Yuan, H.-L. Jiang, and K. T. Law, Phys. Rev. B **93**, 180501 (2016).
[16] N. F. Q. Yuan, K. F. Mak, and K. T. Law, Phys. Rev. Lett. **113**, 097001 (2014).
[17] P. A. Frigeri, D. F. Agterberg, A. Koga, and M. Sigrist, Phys. Rev. Lett. **92**, 097001 (2004).
[18] X. Zhang, Q. Liu, J.-W. Luo, A. J. Freeman, and A. Zunger, Nat. Phys. **10**, 387 (2014).
[19] J. M. Riley, F. Mazzola, M. Dendzik, M. Michiardi, T. Takayama, L. Bawden, C. Granerød, M. Leandersson, T. Balasubramanian, M. Hoesch *et al.*, Nat. Phys. **10**, 835 (2014).
[20] X.-Y. Dong, J.-F. Wang, R.-X. Zhang, W.-H. Duan, B.-F. Zhu, J. O. Sofo, and C.-X. Liu, Nat. Commun. **6**, 8517 (2015).
[21] A. M. Jones, H. Yu, J. S. Ross, P. Klement, N. J. Ghimire, J. Yan, D. G. Mandrus, W. Yao, and X. Xu, Nat. Phys. **10**, 130 (2014).
[22] Q. Liu, Y. Guo, and A. J. Freeman, Nano Lett. **13**, 5264 (2013).
[23] M. Sigrist, D. F. Agterberg, M. H. Fischer, J. Goryo, F. Loder, S.-H. Rhim, D. Maruyama, Y. Yanase, T. Yoshida, and S. J. Youn, J. Phys. Soc. Jpn. **83**, 061014 (2014).
[24] J. Goryo, M. H. Fischer, and M. Sigrist, Phys. Rev. B **86**, 100507 (2012).
[25] M. H. Fischer, F. Loder, and M. Sigrist, Phys. Rev. B **84**, 184533 (2011).
[26] S. J. Youn, M. H. Fischer, S. H. Rhim, M. Sigrist, and D. F. Agterberg, Phys. Rev. B **85**, 220505 (2012).
[27] S. Nakosai, Y. Tanaka, and N. Nagaosa, Phys. Rev. Lett. **108**, 147003 (2012).
[28] A. Larkin and I. Ovchinnikov, Sov. Phys. JETP **20**, 762 (1965).
[29] P. Fulde and R. A. Ferrell, Phys. Rev. **135**, A550 (1964).
[30] D. Xiao, G.-B. Liu, W. Feng, X. Xu, and W. Yao, Phys. Rev. Lett. **108**, 196802 (2012).
[31] L. Fu and E. Berg, Phys. Rev. Lett. **105**, 097001 (2010).
[32] See Supplemental Material at http://link.aps.org/supplemental/10.1103/PhysRevLett.118.087001, for details of the derivation for Landau-Ginzburg free energy, the Green function and superconductivity susceptibility, critical temperature for different types of pairing with and without external magnetic fields, the phase diagram and the possible experimental detection, which includes Ref. [33].
[33] K. V. Samokhin, Phys. Rev. B **70**, 104521 (2004).
[34] L. Fu, Phys. Rev. B **90**, 100509 (2014).
[35] K. Ueda and T. M. Rice, Phys. Rev. B **31**, 7114 (1985).
[36] R. Casalbuoni and G. Nardulli, Rev. Mod. Phys. **76**, 263 (2004).
[37] M. Houzet and A. Buzdin, Phys. Rev. B **63**, 184521 (2001).
[38] D. F. Agterberg and R. P. Kaur, Phys. Rev. B **75**, 064511 (2007).
[39] H.-D. Chen, O. Vafek, A. Yazdani, and S.-C. Zhang, Phys. Rev. Lett. **93**, 187002 (2004).
[40] R. Soto-Garrido and E. Fradkin, Phys. Rev. B **89**, 165126 (2014).
[41] O. Dimitrova and M. V. Feigelman, Phys. Rev. B **76**, 014522 (2007).
[42] R. P. Kaur, D. F. Agterberg, and M. Sigrist, Phys. Rev. Lett. **94**, 137002 (2005).
[43] K. Michaeli, A. C. Potter, and P. A. Lee, Phys. Rev. Lett. **108**, 117003 (2012).
[44] K. Yang and D. F. Agterberg, Phys. Rev. Lett. **84**, 4970 (2000).
[45] D. Efimkin and Y. E. Lozovik, J. Exp. Theor. Phys. **113**, 880 (2011).
[46] B. Seradjeh, Phys. Rev. B **85**, 235146 (2012).